Journal of Nuclear Materials 465 (2015) 784–792

Contents lists available at ScienceDirect

Journal of Nuclear Materials

journal homepage: www.elsevier.com/locate/jnucmat

Microstructural evolution of a uranium-10 wt.% molybdenum alloy for nuclear reactor fuels

A.J. Clarke*, K.D. Clarke, R.J. McCabe, C.T. Necker, P.A. Papin, R.D. Field, A.M. Kelly, T.J. Tucker, R.T. Forsyth, P.O. Dickerson, J.C. Foley, H. Swenson, R.M. Aikin, Jr, D.E. Dombrowski

Los Alamos National Laboratory, Materials Science and Technology Division, Los Alamos, NM 87545, United States

ARTICLE INFO

Article history:
Received 25 February 2015
Received in revised form
11 June 2015
Accepted 1 July 2015
Available online 7 July 2015

Keywords:
Uranium
Uranium alloys
Fuels and fuel elements
Electron microscopy
Processing
homogenization
Segregation

ABSTRACT

Low-enriched uranium-10 wt.% molybdenum (LEU-10wt.%Mo) is of interest for the fabrication of monolithic fuels to replace highly-enriched uranium (HEU) dispersion fuels in high performance research and test reactors around the world. In this work, depleted uranium-10 wt.%Mo (DU-10wt.%Mo) is used to simulate the solidification and microstructural evolution of LEU-10wt.%Mo. Electron backscatter diffraction (EBSD) and complementary electron probe microanalysis (EPMA) reveal significant microsegregation present in the metastable γ-phase after solidification. Homogenization is performed at 800 and 1000 °C for times ranging from 1 to 32 h to explore the time–temperature combinations that will reduce the extent of microsegregation, as regions of higher and lower Mo content may influence local mechanical properties and provide preferred regions for γ-phase decomposition. We show for the first time that EBSD can be used to qualitatively assess microstructural evolution in DU-10wt.%Mo after homogenization treatments. Complementary EPMA is used to quantitatively confirm this finding. Homogenization at 1000 °C for 2–4 h may the regions that contain 8 wt.% Mo or lower, whereas homogenization at 1000 °C for longer than 8 h effectively saturates Mo chemical homogeneity, but results in substantial grain growth. The appropriate homogenization time will depend upon additional microstructural considerations, such as grain growth and intended subsequent processing. Higher carbon LEU-10wt.%Mo generally contains more inclusions within the grains and at grain boundaries after solidification. The effect of these inclusions on microstructural evolution (e.g. grain growth) during homogenization and as potential γ-phase decomposition nucleation sites is unclear, but likely requires additional study.

Published by Elsevier B.V.

1. Introduction

The United States Department of Energy (DOE), National Nuclear Security Administration's (NNSA) Materials Management and Minimization Reactor Conversion program is actively working to convert civilian research and test reactors from the use of highly-enriched uranium (HEU) fuel to low-enriched uranium (LEU) fuel to support nonproliferation and HEU minimization policies. DOE NNSA provides governments and facilities around the world with technical and economic assistance for conversion. If suitable LEU fuels are not available, the program contributes to the development of new LEU fuels. To date, DOE NNSA has converted or verified the shutdown of 87 research reactors worldwide, including 20 domestic facilities. Of the remaining domestic research reactors, five U.S. high performance research reactors (HPRRs) will require a new high density LEU fuel and fabrication capability, which is currently under development. Simply substituting LEU for HEU into existing and qualified HEU dispersion fuel designs will not meet the uranium loading requirements for operating these HPRRs. Affected reactors include the Advanced Test Reactor (ATR) at Idaho National Laboratory, the High Flux Isotope Reactor (HFIR) at Oak Ridge National Laboratory, the University of Missouri Research Reactor (MURR), the Massachusetts Institute of Technology Reactor (MITR), and the Department of Commerce National Institute of Standards and Technology NBSR research reactor. To maintain performance requirements, DOE NNSA is developing high-density monolithic, rather than dispersion, fuel plates that contain low-enriched

* Corresponding author.
E-mail address: aclarke@lanl.gov (A.J. Clarke).

http://dx.doi.org/10.1016/j.jnucmat.2015.07.004
0022-3115/Published by Elsevier B.V.

uranium-10 wt.% molybdenum (LEU-10wt.%Mo) alloy foils clad with 6061 aluminum (Al).

Uranium (U) is alloyed with molybdenum (Mo) to stabilize the high-temperature gamma (γ) phase at room temperature. During U-10wt.%Mo solidification, chemical microsegregation develops. The first γ-phase solid is enriched with Mo solute, followed by the formation of solid that is progressively leaner in Mo solute. Thus, the resulting solidification structure exhibits compositional inhomogeneity at the micro-scale (sub-grain scale). The eutectoid reaction $\gamma \rightarrow U_2Mo\ (\gamma') + \alpha$-U occurs at 550 °C at the U-10wt.%Mo composition, according to the equilibrium U–Mo phase diagram [1]. The γ-phase is body-centered-cubic (bcc) with a lattice parameter of 0.349 nm [1,2]. The U_2Mo phase is tetragonal with lattice parameters of a = b = 0.3427 and c = 0.9834 nm [1,2], but may also be thought of as an ordered version of the bcc γ-phase [2]. The α-U phase is orthorhombic, with lattice parameters of a = 0.28536, b = 0.58698, and c = 0.49555 nm [1,2]. The high-temperature, bcc γ-phase is easily retained as a metastable phase at room temperature, provided a critical cooling rate is achieved [3].

The isotropic bcc γ-phase thus provides swelling and oxidation resistance and the required mechanical properties for HPRR LEU-Mo foils [4], although U–Mo alloys containing substantial levels of Mo, such as 10 wt.%, may be susceptible to stress corrosion cracking [3,4]. Compositionally homogeneous γ-phase should exhibit isotropic properties [5]. However, local Mo variations may influence local (micro-scale) strengths and strains during foil fabrication processes such as rolling and forming, as strength increases significantly with Mo content (approximately 67 MPa per 1 wt.% Mo) [4]. Metastable γ-phase regions with lower Mo content are also more likely to decompose into the $U_2Mo\ (\gamma') + \alpha$-U phases during slow cooling, aging, and/or thermal processing (e.g., during annealing heat treatments or the hot-isostatic press (HIP) cycle – 560 °C, 1.5 h, 103 MPa – used to bond the 6061 Al cladding), potentially resulting in anisotropic mechanical properties and thermal expansion. The isothermal initiation time for α-U formation at 500 °C is reduced from nearly 10 h in U-10wt.%Mo to less than 1 h in U-8wt.%Mo [6–14].

Aging U-10wt.%Mo at temperatures greater than around 375 °C results in γ-phase decomposition into lamellar α-U and enriched γ, primarily at γ grain boundaries and inclusions [7]. Precipitation of acicular α-U may also occur at high temperatures [7]. Below the eutectoid temperature, the enriched γ phase of the lamellar product will eventually order and form the γ' phase [7]. Interestingly, the reverse reaction ($U_2Mo + \alpha$-U $\rightarrow \gamma$) reportedly occurs under irradiation, resulting in stabilization of the γ-phase and a reduction in the amount of anisotropic α-U present in the microstructure during reactor service [8]. This suggests control of γ-phase decomposition is most critical during processing. Below approximately 375 °C, decomposition begins by the formation of γ' [7].

To produce LEU-10wt.%Mo monolithic fuel plates, as-cast U-10wt.%Mo is subsequently hot- and cold-rolled to foils ranging from approximately 0.25 to 2.00 mm in thickness. Zirconium (Zr) co-rolling is also performed to create a diffusion barrier layer between the foil and the HIP-bonded 6061 Al cladding. Some fuel plates (MURR, HFIR, and ATR) are then cold-formed after HIP-bonding. The microstructural evolution of the foil during processing may be important, as cracking, preferential deformation, localized residual stresses, large inclusions, or differences in local phase stability may contribute to failure during fuel plate fabrication [15–20] or in-service. To date, apart from large inclusions that have been problematic during processing [16], specific microstructural characteristics have not been linked to in-service failures. The goal of this work was to start with an as-cast depleted U-10wt.% Mo (DU-10wt.%Mo) solidification structure and to study the microstructural evolution that occurs during homogenization to provide insight into time–temperature combinations that reduce compositional inhomogeneity in the γ-phase and establish a more optimal starting microstructure for subsequent processing. Limited homogenization studies for U-10wt.%Mo alloys are available, but Coughlen et al. reported full homogenization (determined by metallographic examination) is reached in as-cast material containing 700 wppm carbon after the following temperature-time combinations: 900 °C-24 h, 1000 °C-12 h, and 1090 °C-6 h [21]. The 1090 °C-6 h homogenization treatment was also reported to cause massive grain growth [21].

2. Experimental

A depleted uranium-10 wt.% molybdenum (DU-10wt.%Mo) alloy casting was made at Los Alamos National Laboratory for subsequent rolling trials of monolithic foils and to simulate the casting and rolling of LEU-10wt.%Mo alloy foils. An objective of the casting process was to minimize species segregation on the macroscopic scale (i.e., from the top to the bottom and the center to the edge of the casting). To achieve this aim, pre-alloying of DU and Mo sheet was performed in a non-consumable electrode arc-melter to make DU-10wt.%Mo buttons. Each button was approximately 2 kg and melted three times to ensure adequate mixing. These arc-melted buttons served as the charge material for the casting. A plate/hot-top graphite mold assembly was used. Plate dimensions (height × width × thickness) were 206 × 155 × 16.5 mm (8.1 × 6.1 × 0.65 inch) and hot-top dimensions were 99 × 188 × 23 mm (3.9 × 7.4 × 0.9 inch), as shown in Fig. 1. Type-YP yttria mold coating was used. Arc-melted DU-10 wt.%Mo buttons were charged and vacuum induction melted. The maximum temperature achieved during the melt was 1450 °C, followed by pouring (by pulling a stopper rod) at 1350 °C into the graphite mold assembly. The thermal conditions in the mold at the time of the pour consisted of a funnel temperature of 1100 °C, the top of the plate mold at 900 °C, and the bottom of the plate mold at 650 °C. After the pour, the furnace was left to cool overnight. Average compositions of the bottom, middle, and top of the center of the casting were 10.52 ± 0.54 wt.% Mo, 10.72 ± 1.12 wt.% Mo, and

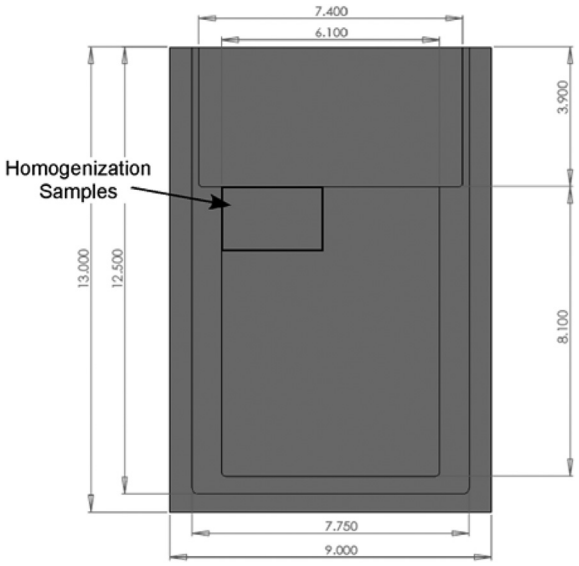

Fig. 1. Drawing of graphite mold used to cast the DU-10wt.%Mo plate. Casting and hot-top dimensions (in inches) and the location of the homogenization samples are shown. The thickness of the cast plate is 0.65 in (16.5 mm) and the thickness of the hot-top is 0.90 in (22.86 mm).

10.47 ± 0.87 wt.% Mo, respectively, based on electron probe microanalysis (EPMA) through-thickness line traces. Similarly, average compositions from the top left edge of the casting were 10.81 ± 0.79 wt.% Mo and 10.64 ± 0.92 wt.% Mo. Thus, no substantial macroscopic Mo segregation existed. The average carbon content of the casting sampled at five locations along the centerline from the bottom to the top was 136 ± 11 wppm from LECO analysis. A value of 160 ± 27 wppm carbon was measured from the upper left quadrant, or the homogenization sample region.

The casting was sectioned for follow-on processing studies, including the homogenization study presented here. The samples for this study came from the upper left corner of the plate casting, from an approximately 45 × 73 × 16.5 mm (1.75 × 2.875 × 0.65 inch) section, located just below the hot-top and spanning from the left edge of the casting to the center, as identified in Fig. 1. Cubes approximately 17 × 13 × 16.5 mm (0.67 × 0.50 × 0.65 inch) were cut for homogenization treatments at 800 °C for 4 and 16 h and at 1000 °C for 1, 2, 4, 8, 16, and 32 h. Cubes were encapsulated in quartz under ultra-high purity argon, given a homogenization treatment, and then ice-water quenched for microstructural analysis with electron microscopy and comparison with the as-cast condition.

DU-10wt.%Mo samples were mounted and then mechanically ground and polished, ending with 1 μm diamond. For electron backscatter diffraction (EBSD), electropolishing at 20–25 V DC in an agitated solution of 45% ethanol, 27% ethylene glycol, and 27% phosphoric acid for approximately 2–5 min was performed with sample rotation every 30 s. Colloidal graphite and copper tape were applied to the non-conducting surfaces of the metallographic mount following electropolishing to prevent sample charging in the scanning electron microscope (SEM). An FEI XL30 ESEM with a TSL/EDAX system was used for EBSD. Automated EBSD scans were performed at 25 kV with a step size of 1 μm, unless otherwise indicated, using TSL OIM™[1] Data Collection software. EBSD crystal orientation results were analyzed with TSL OIM™ Analysis software. Data clean-ups were performed in some instances.

EPMA was performed on as-cast and homogenized DU-10wt.% Mo microstructures in the as-mechanically-polished condition. A CAMECA SX100, operating at 15 KV and 30 nA with X-PHI matrix correction, was used. The diffracting crystal for both elements (U and Mo) was a PET crystal.

As-cast DU-10wt.%Mo microstructures were compared to as-cast LEU-10wt.%Mo ones to qualitatively compare the effects of higher inclusion content and carbon level [15,16,19,20,22,23]. The 248 × 203 × 5.6 mm (9.75 × 8.0 × 0.220 in) LEU-10wt.%Mo casting, which doesn't include the hot-top [16], was produced at the Y-12 National Security Complex and had a carbon content of approximately 800 wppm. Light optical microscopy (LOM) was performed on polished and etched, as-cast DU-10wt.%Mo and LEU-10wt.%Mo samples. Electrolytic etching was performed with 5% phosphoric and/or 10% oxalic solutions. The FEI XL30 ESEM with a TSL/EDAX system was operated at 20 kV with a spot size of 5 to obtain SEM images and to acquire energy-dispersive x-ray spectroscopy (EDS) elemental maps of specific microstructural features in an LEU-10wt.%Mo foil.

3. Results

Although casting of the plate for this homogenization study did not yield significant macrosegregation, example EBSD results from an earlier DU-10wt.%Mo casting are shown in Fig. 2a–c that highlight microscopic chemical segregation in the metastable γ-phase after solidification. An inverse pole figure (IPF) map is shown in Fig. 2a, along with a corresponding standard cubic stereographic projection, revealing the crystallographic orientations of the grains. An image quality map (IQ) is shown in Fig. 2b. In this representation, the brighter regions correspond to areas where higher quality diffraction patterns were obtained. The IQ map highlights patterns that exist within the grains and appear to correlate with the microscopic chemical segregation produced by dendritic solidification. The IPF map is superimposed together with the IQ map in Fig. 2c to simultaneously show both orientation and IQ, which highlights dendrites associated with individual grains.

To make DU-10wt.%Mo foils, the as-cast material must be rolled. Fig. 2d–i shows example EBSD results after hot rolling (salt bath at 670 °C, plate temperature >650 °C) or hot rolling and annealing (700 °C, 1 h) trials of an earlier casting. A typical bcc rolling texture is produced, and partially or fully recrystallized grains form within the bands revealed by IQ. The bands are associated with deformation, but are also convoluted with the microsegregation from solidification, which may affect mechanical response during subsequent cold-rolling and forming operations. As hot rolled samples, Fig. 2d–f, show bands of partially recrystallized grains, which may occur in regions of lower Mo content, have lower strength, and therefore accumulate more strain, resulting in faster recrystallization kinetics. After hot rolling and annealing, full recrystallization is achieved. The results shown in Fig. 2 motivated further study of as-cast and homogenized DU-10wt.%Mo microstructures with EBSD and EPMA to explore the time–temperature combinations that would reduce micro-scale chemical inhomogeneity prior to subsequent hot- and cold-rolling.

To confirm the patterns in the EBSD IQ and IPF+IQ maps are indeed associated with the microsegregation from solidification, hardness indents were used to mark a grain in a homogenization sample from the casting made for this study, as shown in Fig. 3. Within this grain, the IPF+IQ maps in Fig. 3a reveal brighter regions. An EPMA trace across the grain, Fig. 3b, and through two of the brighter regions shown by EBSD confirms that these regions are associated with higher Mo contents, Fig. 3c, compared to the darker, lower IQ regions within the grain.

An EBSD IPF+IQ map of the as-cast solidification structure of the casting produced for this study is shown in Fig. 4a. Patterns typical of dendritic solidification with brighter regions corresponding to higher Mo contents and significant microsegregation are clearly revealed. EBSD IPF+IQ maps of the microstructure after homogenization at 800 °C for 4 and 16 h are shown in Fig. 4b and c, respectively. Note that the grain in Fig. 3 is shown in the far right of Fig. 4c. With increasing homogenization time, the patterns within the grains become more difficult to distinguish. EMPA traces across the through-thickness of the casting are shown in Fig. 4d–f for the as-cast and 800 °C homogenization conditions. The average composition determined for the as-cast condition is 10.64 ± 0.92 wt.% Mo. After homogenization for 4 and 16 h at 800 °C, the average compositions are 10.44 ± 0.78 wt.% Mo and 10.26 ± 0.57 wt.% Mo, respectively, showing that increasing homogenization time results in increasing chemical homogeneity. The EPMA results also qualitatively agree with the decreases in contrast with increasing homogenization time in the EBSD IPF+IQ maps.

Homogenization was also performed at 1000 °C for 1, 2, 4, 8, 16, and 32 h. EBSD IPF+IQ maps and EPMA through-thickness composition traces are provided in Fig. 5. As homogenization time increases, the brighter regions within the grains in the IPF+IQ maps begin to disappear, becoming difficult to identify after 8 h of homogenization. The average composition after 1 h at 1000 °C from EPMA is 10.26 ± 0.68 wt.% Mo, which progresses to 10.22 ± 0.11 wt.% Mo after 32 h. A summary of the EPMA results after homogenization at 800 and 1000 °C is provided in Table 1. The

[1] OIM is a trademark AMETEK, Inc.

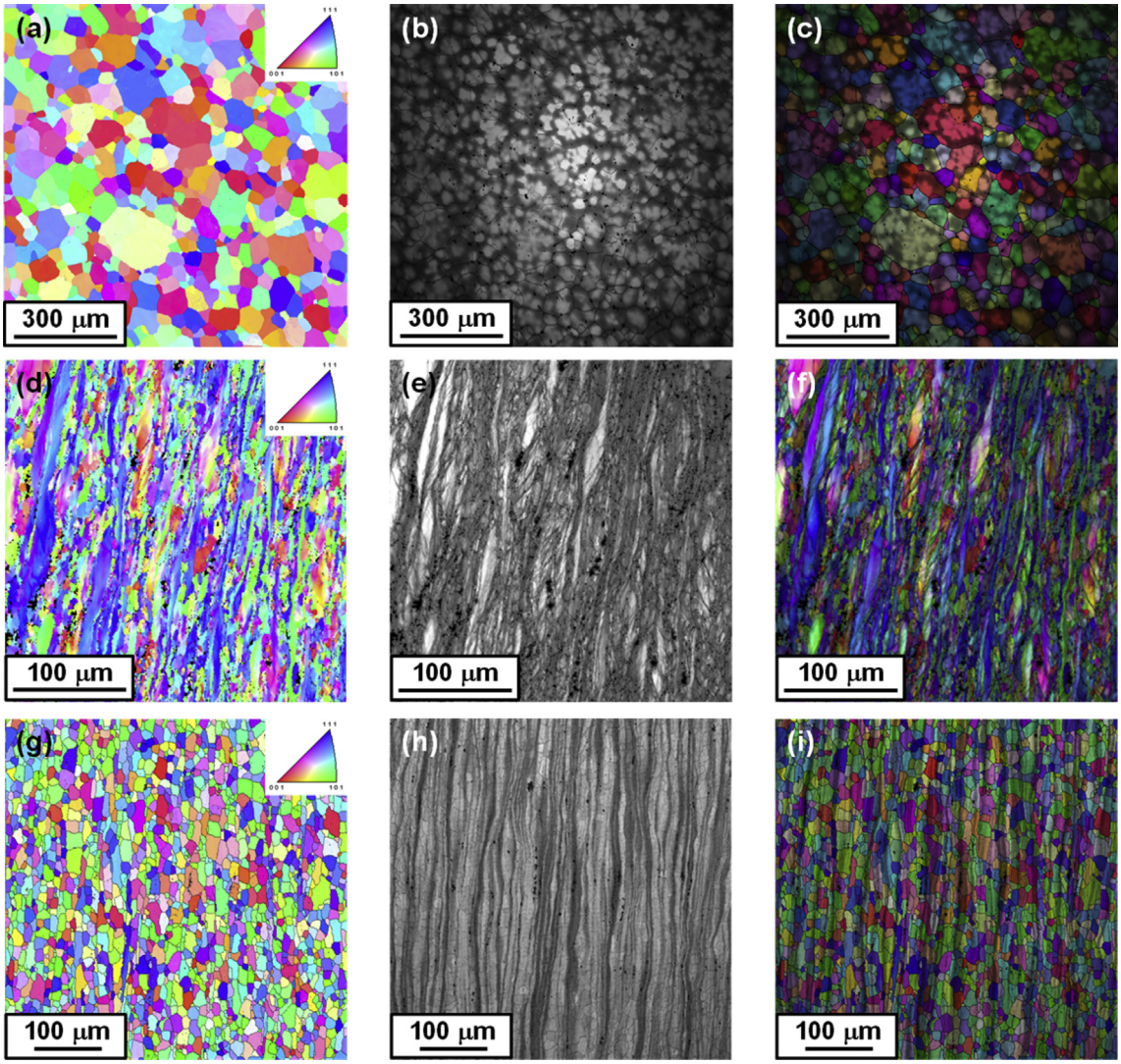

Fig. 2. (a) An EBSD inverse pole figure (IPF) map and corresponding standard cubic stereographic projection color legend showing γ-phase orientations in the early DU-10wt.%Mo casting, (b) an EBSD image quality (IQ) map of the region in (a), and (c) the IPF map in (a) superimposed with the IQ map in (b). (d) An EBSD IPF map of DU-10wt.%Mo after hot rolling at approximately 650 °C, (e) an EBSD IQ map highlighting banding, and (f) the IPF map in (d) superimposed with the IQ map in (e). (g) An EBSD IPF map of DU-10wt.%Mo recrystallized grains after hot rolling at approximately 650 °C and annealing at 700 °C, (h) an EBSD IQ map highlighting banding, and (i) the IPF map in (g) superimposed with the IQ map in (h). 10 pt and 3 pt dilation clean-ups were used for (c) and (i), respectively, and 5° boundaries are shown. A neighbor confidence index (CI) correlation clean-up was performed for (f); less than 10% of the points were changed. (For interpretation of the references to colour in this figure legend, the reader is referred to the web version of this article.)

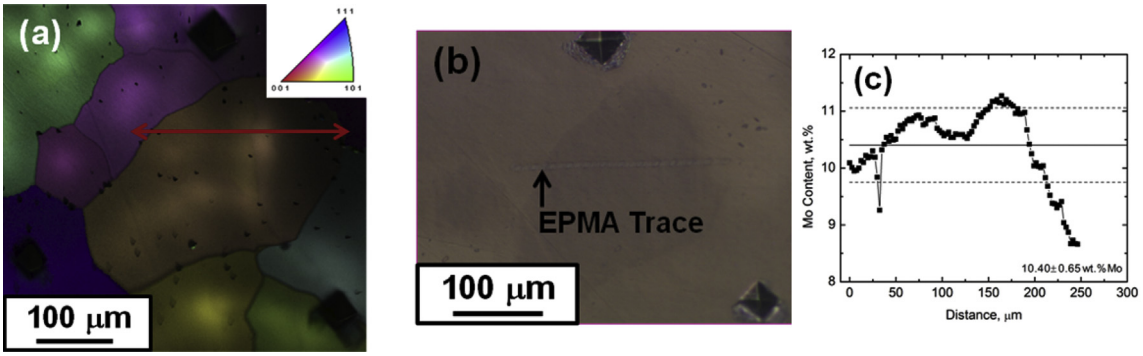

Fig. 3. (a) An EBSD IPF+IQ map of a γ-phase grain with bright regions and marked by hardness indents in a homogenization sample (800 °C, 16 h) from this study. (b) An EPMA composition trace across the grain that reveals the bright regions in (a) are associated with higher Mo contents. (c) the EPMA composition trace in (b). A 10 pt dilation clean-up was used in (a).

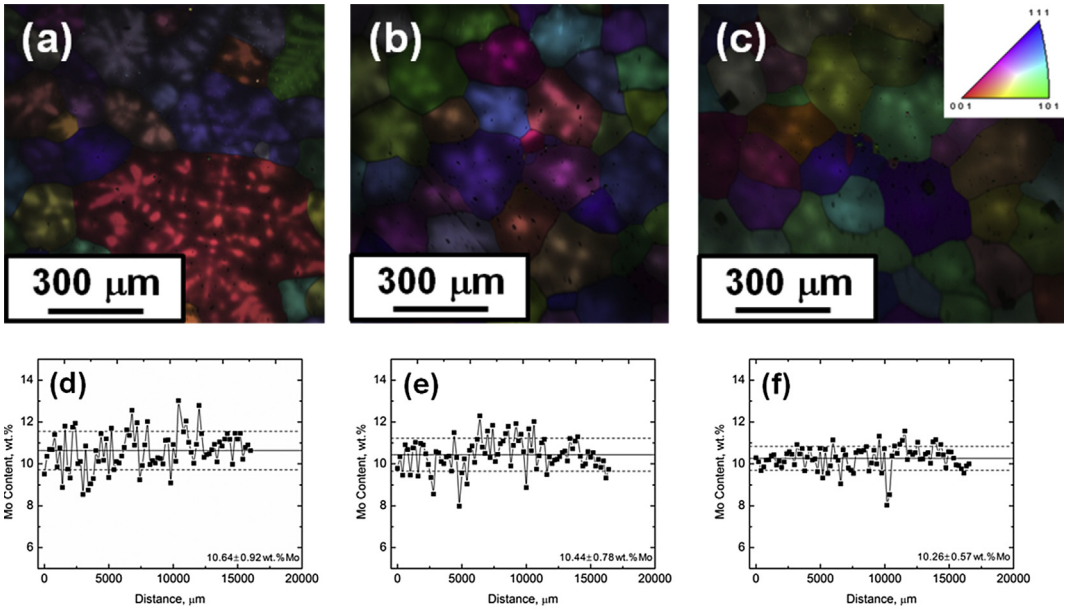

Fig. 4. (a) An EBSD IPF+IQ map of the as-cast microstructure, (b) an EBSD IPF+IQ map after homogenization at 800 °C for 4 h, and (c) an EBSD IPF+IQ map after homogenization at 800 °C for 16 h. (d) A through-thickness EPMA trace and the average composition of the as-cast microstructure and (e, f) EMPA composition traces after homogenization at 800 °C for 4 and 16 h, respectively. Note that the grain in Fig. 3 is shown in the far right of (c). 10 pt dilation clean-ups were used for (a), (b), and (c).

average compositions after homogenization at 4 and 16 h show that 1000 °C reduces Mo variations within the microstructure more quickly than 800 °C, as expected. Increasing homogenization time at 1000 °C also qualitatively results in significant grain growth, as shown in Fig. 5, whereas unambiguous grain growth is not evident in Fig. 4 after homogenization at 800 °C.

4. Discussion

EBSD IPF+IQ maps qualitatively reveal the patterns that develop during dendritic solidification within DU-10wt.%Mo grains. EPMA confirms that the brighter regions in these maps correspond to regions with higher Mo content. Chemical inhomogeneity of the metastable γ-phase solidification structure at the microscopic scale will likely translate throughout any downstream wrought processing, unless homogenization is performed, and will result in varying local mechanical properties. Mo variations may also influence local γ-phase stability. For example, lower Mo regions may experience accelerated decomposition at elevated temperatures. Fig. 6 shows high resolution IPF, IQ, and confidence index (CI) maps captured at a 0.1 μm step size of lamellar structure in rolled and HIPped DU-10wt.%Mo [19]. Similar lamellar structures at grain boundaries in lower Mo regions in DU-10wt.%Mo were reported by Nyberg et al. in the as-cast condition, after homogenization at 800 °C for 24 h, and after homogenization and elevated temperature mechanical testing, which may have reduced the flow stress [23]. Lamellar structure was not observed after homogenization at 1000 °C for 16 h, however [23].

Based upon microstructural examinations after homogenization at 800 and 1000 °C, 1000 °C appears to be more effective at maximizing chemical homogeneity in times relevant for manufacturing. Recommendation of an optimized homogenization treatment depends upon two criteria: 1) minimizing extremely low Mo regions to avoid accelerated γ-phase decomposition and the formation of α-U during subsequent processing, such as annealing or hot-isostatic pressing (8 wt.% Mo and lower, for example, results in γ-phase decompositions at times and temperatures similar to those used for the HIP bonding cycle), and 2) substantially reducing the extent of Mo variation to minimize microstructural effects during deformation processing. To achieve the first, homogenization at 1000 °C for 2–4 h appears to sufficiently eliminate extremely low Mo (<8 wt.%) regions. To achieve the second, homogenization at 1000 °C for more than 8 h significantly reduces the chemical inhomogeneity, which is in agreement with the values determined metallographically by Coughlen et al. [21]. The appropriate time may also depend upon additional considerations, such as grain growth that may occur with increasing homogenization time. For DU-10wt.%Mo rolled fuel foils, grain growth may not be a significant concern, as subsequent rolling and heat-treatment may be performed to reduce the grain size and promote the formation of recrystallized grains. The extent of grain growth acceptable during homogenization has not been determined, but will depend upon the amount of work imparted during subsequent rolling processing. If sufficient reduction is imparted during rolling, a fine, recrystallized grain size may be achieved in the final fuel foil. Further work is recommended to understand the relationship between the as-cast thickness, homogenization, and subsequent rolling to better understand acceptable processing windows.

An important difference between the DU-10wt.%Mo investigated here and the LEU-10wt.%Mo typically used to manufacture foils is the carbon content. This DU-10wt.%Mo casting was made with low carbon DU feedstock, with carbon levels ranging from 100 to 150 wppm, whereas other feedstocks and the feedstock frequently used to make LEU-10wt.%Mo may have substantially higher carbon levels. For example, Nyberg et al. reported a carbon level of approximately 900 wppm in their DU-10wt.%Mo used in a recent homogenization and mechanical property assessment [23], and Coughlen et al. reported 700 wppm [21]. These values are more representative of typical LEU-10wt.%Mo used for fuel foil manufacture.

Example LOM images of as-cast DU-10wt.%Mo and LEU-10wt.% Mo are shown in Fig. 7. The microstructures in Fig. 7a–c were etched to reveal the dendritic solidification structure within the grains, whereas the microstructures in Fig. 7d–f highlight the inclusions in higher carbon LEU-10wt.%Mo. The dendrite contrast observed in Fig. 7a–c is thought to be due to the dependence of

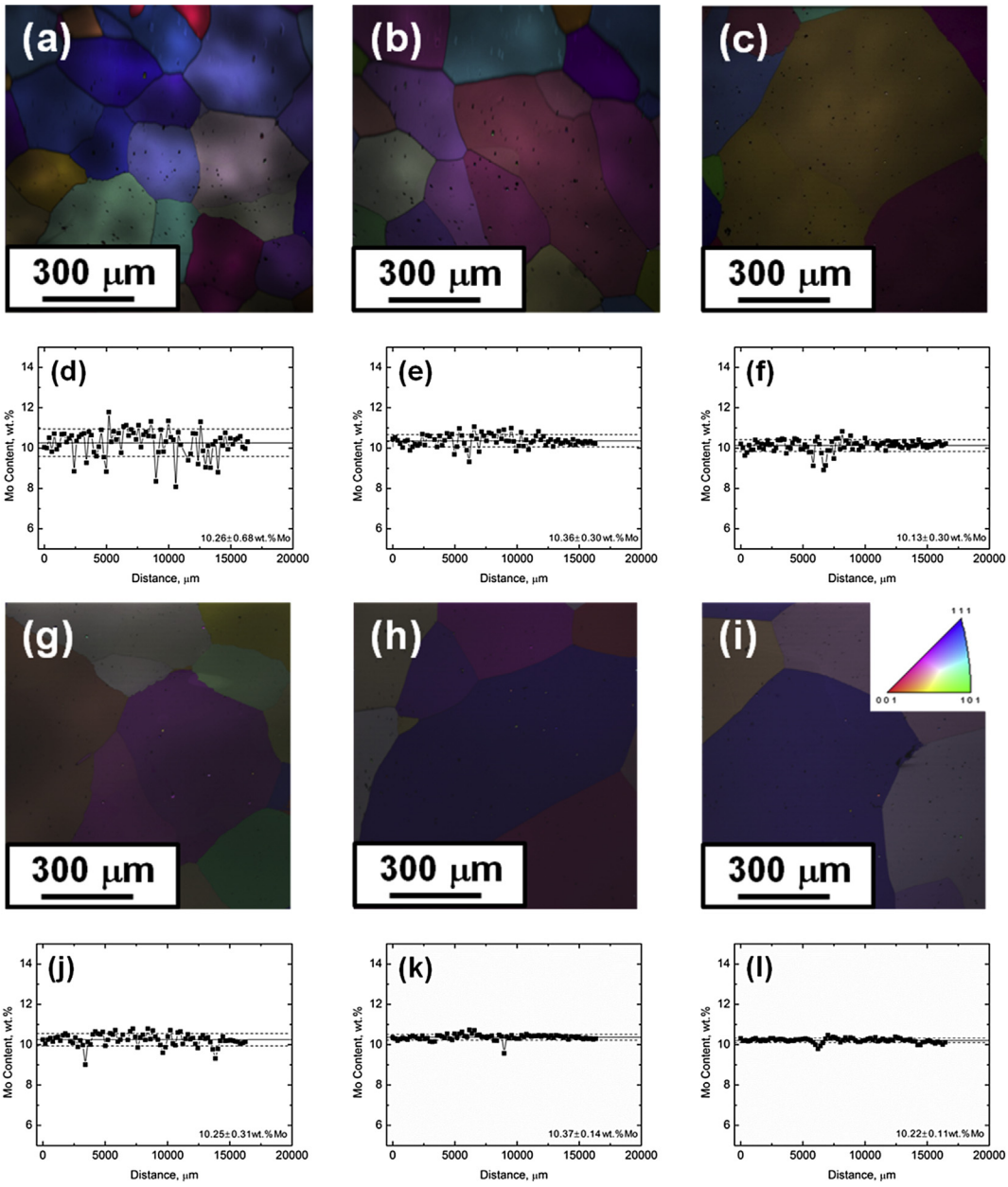

Fig. 5. An EBSD IPF+IQ map after homogenization at 1000 °C for (a) 1 h, (b) 2 h, (c) 4 h, (g) 8 h, (h) 16 h, and (i) 32 h, and EPMA through-thickness composition traces after (d) 1 h, (e) 2 h, (f) 4 h, (j) 8 h, (k) 16 h, and (l) 32 h. 10 pt dilation clean-ups were used for (a), (b), (c), (g), (h), and (i).

oxidation rate on Mo concentration. Regions with higher Mo concentration oxidize more slowly than regions with lower Mo concentration. This contrast effect is also likely the primary cause of the concentration dependence in the EBSD IQ maps. Despite our best efforts to perform EBSD directly following electropolishing of the surface, some oxidation occurs in the several minutes necessary to load the sample for EBSD, and different thicknesses of oxide on the surface may directly affect the IQ. The different grain sizes for these two microstructures are likely associated with the different casting conditions used to make these two castings and different inclusion contents.

Table 1
A summary of EPMA results after homogenization at 800 and 1000 °C.

Homogenization temperature, °C	Homogenization time, h	Average composition, wt.% Mo
0	0	10.64 ± 0.92
800	4	10.44 ± 0.78
800	16	10.26 ± 0.57
1000	1	10.26 ± 0.68
1000	2	10.36 ± 0.30
1000	4	10.13 ± 0.30
1000	8	10.25 ± 0.31
1000	16	10.37 ± 0.14
1000	32	10.22 ± 0.11

The carbide inclusions in the LEU-10wt.%Mo tend to form patterns within the grains. Also, inclusions often exist at the grain boundaries in LEU-10wt.%Mo, as shown in Fig. 7d–f. The role of increased inclusion content in high carbon LEU-10wt.%Mo during homogenization is unclear, as they may influence grain growth or perhaps even alter local chemistry. For example, our low-carbon DU-10wt.%Mo results show significant grain growth after homogenization at 1000 °C for 4 h, whereas Coughlen et al. observed grain growth after 6 h at 1090 °C in high-carbon U-10wt.%Mo [21], suggesting different kinetics. Inclusions may also serve as nucleation

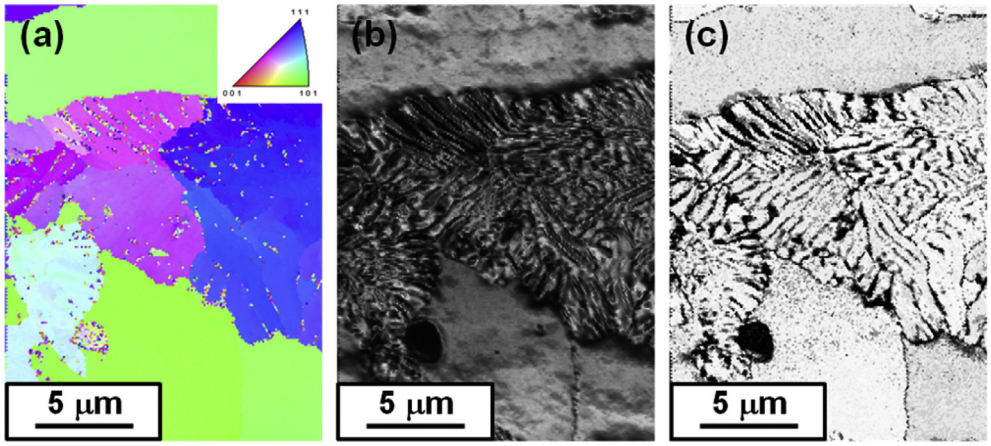

Fig. 6. (a) IPF, (b) IQ, and (c) confidence index (CI) maps captured at a 0.1 μm step size of lamellar structure in rolled and HIPped DU-10wt.%Mo.

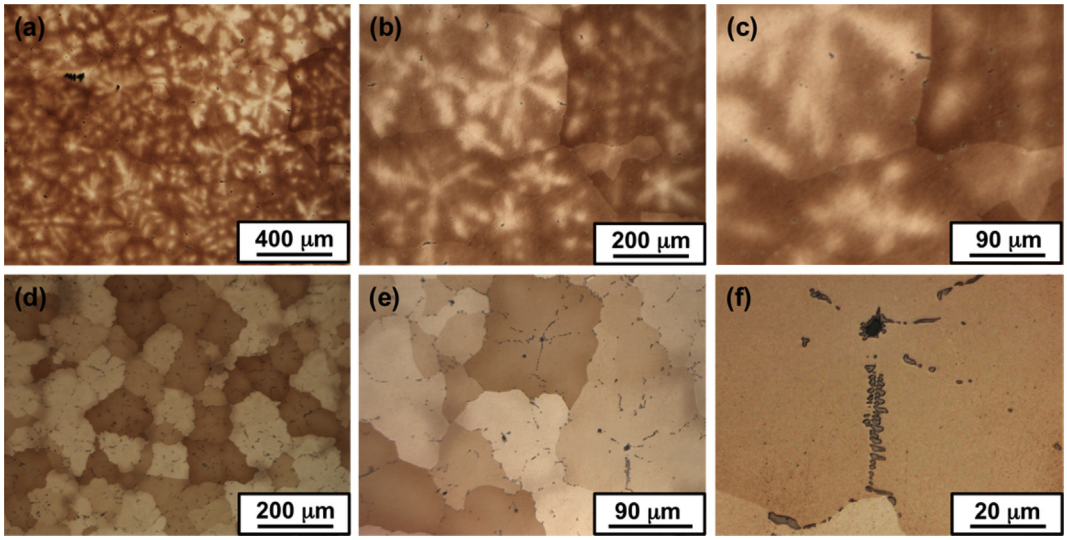

Fig. 7. (a), (b), and (c) Light optical microscopy (LOM) of DU-10wt.%Mo (nominally 100 to 150 wppm carbon), etched to reveal the dendritic solidification structure within the grains and (d), (e), and (f) LOM of LEU-10wt.%Mo (800 wppm carbon), etched to highlight inclusions within the grains and at grain boundaries.

sites for γ-phase decomposition [7,23]. Especially large inclusions, such as those with complex chemical variations shown in Figs. 8 and 9 in rolled LEU-10wt.%Mo, may result in poor mechanical performance during downstream wrought processing [16]. It is unclear how these large inclusions are introduced during casting, but they are observed in high-carbon LEU-10wt.%Mo.

Future rolling studies of homogenized microstructures of low-carbon alloys, e.g. 2 h (small grains) and 16 h (larger grains with significantly reduced Mo segregation) at 1000 °C, should be performed to determine the influence of reduced Mo segregation and grain size on microstructural evolution. Further understanding of the role of inclusions during processing is also needed. Studies with controlled carbon content variations may also be warranted.

5. Conclusions

Complementary microscopy techniques were used to examine the as-cast condition and microstructural evolution in DU-10wt.% Mo after homogenization at 800 °C for 4 and 16 h and 1000 °C for 1, 2, 4, 8, 16, and 32 h. Results are discussed in the context of LEU-10wt.%Mo, which is of interest for the fabrication of monolithic fuels for high performance research and test reactors. The results from this work lead to the following important microstructure/processing conclusions:

1. Solidification of DU-10wt.%Mo results in significant Mo microsegregation in the metastable γ-phase, which may translate throughout downstream wrought processing and affect the final microstructure. Regions of higher and lower Mo content may influence local mechanical properties and provide preferred regions for γ-phase decomposition.
2. EBSD IPF+IQ maps reveal solidification patterns within the grains of DU-10wt.%Mo microstructures. These maps may be used to qualitatively assess Mo variations introduced by processing (e.g., homogenization) over large areas. This finding is confirmed by complementary EPMA.
3. EPMA was used to quantitatively assess the extent of homogenization in DU-10wt.%Mo. Homogenization at 1000 °C for 2 or 4 h was shown to effectively eliminate the regions that contain 8 wt.% Mo or lower, whereas homogenization at 1000 °C for longer than 8 h saturates the chemical homogeneity for processing-relevant times. The appropriate homogenization time will depend upon microstructural

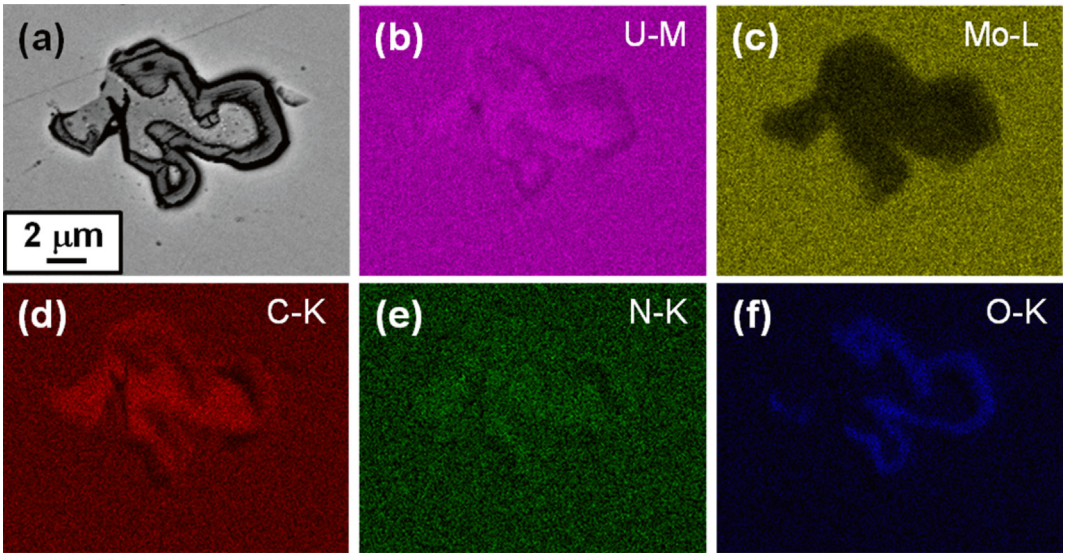

Fig. 8. (a) Scanning electron microscopy (SEM) image of a large inclusion in rolled LEU-10wt.%Mo and (b) uranium, (c) molybdenum, (d) carbon, (e) nitrogen, and (f) oxygen maps obtained with energy dispersive spectroscopy (EDS).

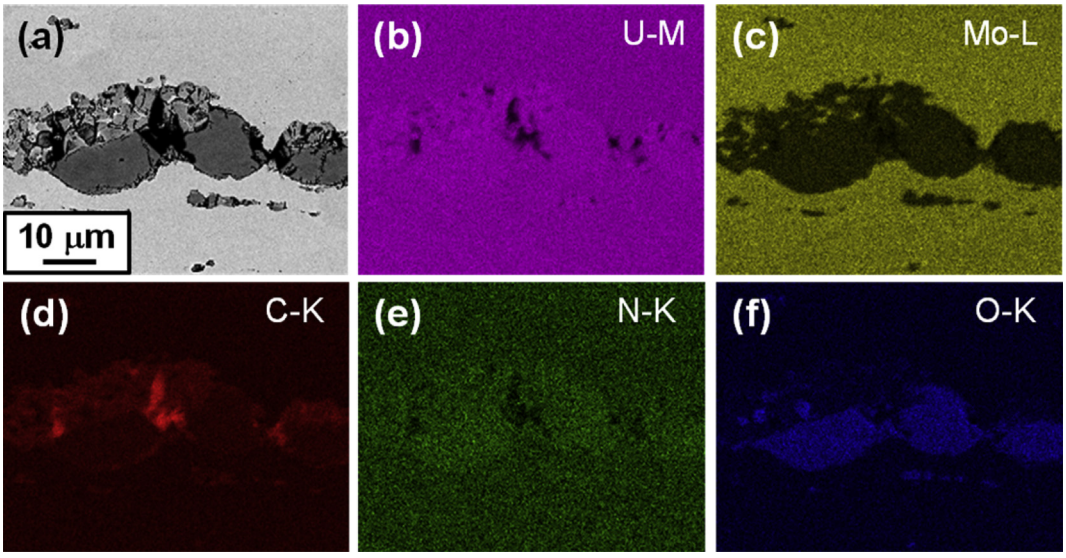

Fig. 9. (a) Scanning electron microscopy (SEM) image of a large inclusion in rolled LEU-10wt.%Mo and (b) uranium, (c) molybdenum, (d) carbon, (e) nitrogen, and (f) oxygen maps obtained with energy dispersive spectroscopy (EDS).

considerations, such as grain growth and the intended subsequent processing.

4. Higher carbon, LEU-10wt.%Mo contains inclusions in patterns within the grains and at grain boundaries after solidification. The effect of these inclusions on microstructural evolution (e.g. grain growth) during homogenization is unknown. Inclusions may serve as nucleation sites for γ-phase decomposition.

Acknowledgments

This work was supported by the U.S. Department of Energy (DOE) National Nuclear Security Administration's Materials Management and Minimization Reactor Conversion Program and Los Alamos National Laboratory, operated by Los Alamos National Security, LLC under Contract No. DE-AC52-06NA25396 for the U.S. DOE. A.J.C. was supported by an Early Career award from the U.S. DOE, Office of Basic Energy Sciences, Division of Materials Sciences and Engineering during the preparation of this manuscript. We also gratefully acknowledge the help of R.E. Hackenberg, R.R. Trujillo, I.P. Cordova, D.R. Guidry, M. Koby, and V.M. Lopez.

References

[1] H. Okamoto, in: second ed., in: T.B. Massalski (Ed.), Mo-U (Molybdenum-Uranium), Binary Alloy Phase Diagrams, vol. 3, 1990, pp. 2682–2683.
[2] E.K. Halteman, Acta Crystallogr. 10 (3) (1957) 166–169.
[3] K.H. Eckelmeyer, Uranium and Uranium Alloys, in: ASM Handbook, vol. 2, ASM International, Materials Park, OH, 1990, pp. 670–682.
[4] D.E. Burkes, R. Prabhakaran, J.-F. Jue, F.J. Rice, Metall. Mater. Trans. A 40A (5) (2009) 1069–1079.
[5] A.S. Wilson, R.E. Rundle, Acta Crystallogr. 2 (2) (1949) 126–127.
[6] P.E. Repas, R.H. Goodenow, R.F. Hehemann, Trans. Am. Soc. Metals 57 (1964) 150–163.
[7] D. Blake, R.F. Hehemann, in: D.A. Colling, J.J. Burke, A.E. Gorum, J. Greenspan (Eds.), Physical Metallurgy of Uranium Alloys, Brook Hill Publishing, Chestnut

Hill, MA, 1976, pp. 89–218.
[8] V.S. Yemel'Yanov, A.I. Yevstyukhin, The Metallurgy of Nuclear Fuel Properties and Principles of the Technology of Uranium, Thorium and Plutonium, Pergamon Press, Oxford, England, 1969, p. 103.
[9] Y. Goldstein, A. Bar-Or, J. Inst. Metals 95 (1967) 17–21.
[10] C.A.W. Peterson, W.J. Steele, S.L. DiGiallonardo, University of California Lawrence Radiation Laboratory Report (1964). UCRL-7824.
[11] S.T. Konobeevskii, N.F. Pravdiuk, K.P. Dubrovin, B.M. Levitiskii, L.D. Panteleev, V.M. Golianov, Soviet J. Atomic Energy 4 (1) (1958) 33–45.
[12] R.J. Van Thyne, D.J. McPherson, Trans. Am. Soc. Metals 49 (1957) 598–621.
[13] V.K. Orlov, V.M. Teplinskaya, N.T. Chebotarev, Atomic Energy 88 (1) (2000) 42–47.
[14] J.M. Fackelmann, A.A. Bauer, D.P. Moak, Battelle Memorial Institute Report, 1969. BMI-X-10264.
[15] A.J. Clarke, K.D. Clarke, D.E. Dombrowski, P.S. Dunn, R.D. Field, J.C. Foley, R.T. Forsyth, D.L. Hammon, A.M. Kelly, D.R. Korzekwa, R.J. McCabe, C.T. Necker, P.A. Papin, D.F. Teter, Los Alamos National Laboratory Report, 2010. LA-UR-10–00195.
[16] D.L. Hammon, K.D. Clarke, D.J. Alexander, P.K. Kennedy, R.L. Edwards, A.N. Duffield, D.E. Dombrowski, Los Alamos National Laboratory Report, 2013. LA-UR-13–24590.
[17] D.W. Brown, D.J. Alexander, K.D. Clarke, B. Clausen, M.A. Okuniewski, T.A. Sisneros, Scr. Mater. 69 (2013) 666–669.
[18] D.W. Brown, M.A. Okuniewski, J.D. Almer, L. Balogh, B. Clausen, J.S. Okasinski, B.H. Rabin, J. Nucl. Mater. 441 (2013) 252–261.
[19] J.C. Foley, A.J. Clarke, K.D. Clarke, P.O. Dickerson, R.M. Dickerson, R.D. Field, R.T. Forsyth, A.M. Kelly, C.T. Necker, P.A. Papin, Los Alamos National Laboratory Report, 2009. LA-UR-09–06439.
[20] S.M. Casey, A.J. Clarke, K.D. Clarke, P.O. Dickerson, R.M. Dickerson, R.D. Field, R.T. Forsyth, T.G. Holesinger, A.M. Kelly, C.T. Necker, P.A. Papin, J.C. Foley, Los Alamos National Laboratory Report, 2010. LA-UR-10–01122.
[21] C.P. Coughlen, P.A. Evans, A.B. Townsend, Union Carbide Corporation, Y-12 Plant, 1969. U.S. Atomic Energy Comission Contract Report No. Y-1696.
[22] A. DeMint, R.J. Dunavant, J. Gooch, T.C. Andes, in: 29th International Meeting on Reduced Enrichment for Research and Test Reactors, RERTR, Prague, Czech Republic, 2007.
[23] E.A. Nyberg, V.V. Joshi, C.A. Lavender, D.M. Paxton, D.E. Burkes, Pacific Northwest National Laboratory Report, 2014. PNNL-23348.